Environmental Research 199 (2021) 111263

Contents lists available at ScienceDirect

Environmental Research

journal homepage: www.elsevier.com/locate/envres

Microwave-assisted green synthesis of fluorescent carbon quantum dots from *Mexican Mint* extract for Fe^{3+} detection and bio-imaging applications

Natarajan Architha [a,1], Murugesan Ragupathi [a,1], Chellappan Shobana [b], Thangasamy Selvankumar [c], Ponnuchamy Kumar [d], Yun Sung Lee [e], Ramakrishnan Kalai Selvan [a,*]

[a] Department of Physics, Bharathiar University, Coimbatore, 641 046, Tamil Nadu, India
[b] Department of Zoology, Kongunadu Arts and Science College (Autonomous), G. N. Mills, Coimbatore, 641 029, India
[c] Department of Biotechnology, Mahendra Arts & Science College, Kalippatti, Namakkal, 637501, Tamil Nadu, India
[d] Department of Animal Health and Management, Alagappa University, Karaikudi, 630 003, India
[e] Faculty of Applied Chemical Engineering, Chonnam National University, Gwangju, 500-757, South Korea

ARTICLE INFO

Keywords:
Carbon quantum dots
Mexican mint
Fe^{3+} detection
Bioimaging

ABSTRACT

Biomass-derived carbon quantum dots have drawn special interest owing to their admirable photostability, biocompatibility, fluorescence, high solubility, sensitivity and environmentally friendly properties. In the present work, the Carbon Quantum Dots (CQDs) was synthesized from the *Plectranthus amboinicus* (Mexican Mint) leaves via the microwave-assisted reflux method. The strong absorption peaks observed from UV–vis spectra at 291 and 330 nm corresponds to the π-π* and n-π* transitions, respectively, reveal the formation of CQDs. The synthesized CQDs showed bright blue fluorescence under UV irradiation with a fluorescence quantum yield of 17% and a maximum emission of 436 nm in the blue region at an excitation wavelength of 340 nm. The HRTEM analysis elucidates that the synthesized CQDs were crystalline and spherical in shape with a particle size of 2.43 ± 0.02 nm. The FT-IR spectroscopy confirms the presence of the different functional groups such as –OH, –CH, C═O and C–O. The chemical composition of CQD was revealed through XPS analysis. The synthesized CQDs were used as a fluorescent probe to detect different metal ions, where high selectivity was obtained for Fe^{3+} ions through quenching phenomenon. The emission intensity of CQD showed a good linear relationship with $R^2 = 0.9111$ with the concentration of Fe^{3+} ions in the range of 0–15 μM. The fluorescence emission of CQD was turned OFF upon the binding of Fe^{3+} ions and turned – ON with the addition of ascorbic acid. With this fluorescent turn ON-OFF behaviour of CQD, the NOT and IMPLICATION logic gates were constructed and studied for different input conditions. The biocompatibility of CQD was tested via MTT assay using MCF7 breast cancer cell line, which revealed that CQD synthesized from the Mexican Mint leaves possess less cytotoxicity. Further, the prepared CQD was applied effectively as fluorescent probes in a cell imaging application.

1. Introduction

Heavy metals create a serious threat to the environment including plants, animals and human beings due to the overexploitation in various industrial and household applications. Hence it is more essential to monitor the concentration of such toxic heavy metal ions in the environment. Among the various metals ions, ferric ion (Fe^{3+}) is one of the most important transition metal ions that play a crucial role in environmental as well as biological systems. Especially, iron is the fundamental structure of haemoglobin, myoglobin and is involved in many enzyme activities. As well as, it plays a prominent role in the chemical and physiological processes of organisms, such as electron transport, nucleic acid synthesis, enzymatic catalysis, and cellular metabolism. Fe^{3+} ions mainly accumulate within liver, spleen and bone marrow cells, bound to ferritin (Murugan et al., 2018). The excess or any insufficiency of Fe^{3+} ions may cause several disorders and diseases, where excess Fe^{3+} ions can cause various types of cancers and decline the functions of organs such as the heart, lungs and pancreas and

* Corresponding author.
E-mail address: selvankram@buc.edu.in (R. Kalai Selvan).
[1] Both the authors have an equal contribution.

https://doi.org/10.1016/j.envres.2021.111263
Received 21 March 2021; Received in revised form 16 April 2021; Accepted 19 April 2021
Available online 1 May 2021

deficiency leads to anaemia in the body. Therefore, it is essential to detect the Fe^{3+} in the environment and human health (Zhang et al., 2019; Suresh Kumar et al., 2019). Thus, it is more necessary to develop a sensitive, selective and safe method to detect Fe^{3+} ion. Among the different detection methods (Theerthagiri et al., 2018; Sedhu et al., 2020; Ramu et al., 2020), fluorescence spectroscopy has drawn increasing attention due to its high sensitivity, simple operation, and excellent reproducibility (Zhao et al., 2020; Wang et al., 2021; Durai-murugan et al., 2021). Similarly, different organic dyes such as porphyrins, indocyanines, boron-dipyrromethene, phthalocyanines, and rhodamines have been used as fluorophores in *in-vitro* and *in-vivo* cell imaging studies. Although these organic dyes have specific chemical structures with excellent optical properties, they are not suitable for long-term and real-time imaging or cell multiplication (Qian et al., 2018). The main limitation of organic dyes is low photobleaching thresholds, poor solubility, small Stokes shift, and broad absorption/emission spectra (Zhu et al., 2019).

In this regard, carbon quantum dots (CQDs) has emerged as an attractive alternative to fluorescence probes for detecting heavy metal ions and cell imaging applications in the recent past because of their unique optical properties (Fan et al., 2019; Wang et al., 2019). CQDs are the new class of carbon nanomaterials along with carbon nanotubes and fullerenes (Chunduri et al., 2016). It is a zero-dimensional nanomaterial having a size of less than 10 nm (Yang et al., 2014; Zhao et al., 2019). It was discovered accidently by Xu et al. (2004) during the purification of single-wall carbon nanotubes. The designed synthesis was carried out first by Sun et al. (2006). Since then, the carbon quantum dots have drawn the increased attention because of their exceptional properties including broad and tunable emission wavelengths, easy surface functionalization, long excitation ranges, good photoluminescence, highly efficient electron-accepting capabilities, high chemical and photostability, good water solubility, low cytotoxicity and low environmental hazard over the other traditional metal-based semiconductor quantum dots (Li et al., 2019). Among these, the excellent photoluminescence and photostability of CQDs have attracted keen attention and find applications in various fields (Yue et al., 2019; Das et al., 2019; Liu et al., 2019; Mittal et al., 2019; Hong et al., 2019; Su et al., 2020. Feng et al., 2019; Lim et al., 2018).

The CQDs can be prepared in two different synthetic ways, namely top-down and bottom-up methods. The bottom-up method refers to the fabrication of CQDs from molecular precursors using microwave irradiation (Bajpai et al., 2019), laser ablation (Singh et al., 2019), ultrasonication (Dehvari et al., 2019), hydrothermal (Naik et al., 2019) methods. Among these, microwave (MW) assisted synthesis is rapid, facile, cost-effective, environmentally friendly. Further, the uniform and selective distribution of microwave energy inside the sample provide high yields, low impurity, and size control with improved safety, better reproducibility, and excellent control over experimental parameters for the preparation of CQDs (Vandarkuzhali et al., 2018; Huang et al., 2018). The major advantage of using microwave heating is the contactless heat transfer to the reactants, which allows the possibility for the reactions to take place in a short time (Vadivel et al., 2016).

The easier availability and increased environmental concerns have made the usage of plant, and other green biomasses as precursors for the synthesis of CQDs. Various sources of biomass precursors including pineapple (Vandarkuzhali et al., 2018), pear (Das et al., 2019), musk melon (Mittal et al., 2019), pumpkin seeds (Qian et al., 2018), milk protein (Bajpai et al., 2019), watermelon (Lu et al., 2018) have been used as the raw materials. However, a very scarce amount of work has been reported on the synthesis of CQDs using leaves of the Mexican Mint (*Plectranthus amboinicus*) plant. *Plectranthus amboinicus*, (Lour.) Spreng. is a perennial herb that belongs to the Lamiaceae family, with a pungent oregano-like flavour and odour. It occurs naturally throughout the tropics and warm regions of Asia, Africa, and Australia. It contains 76 volatiles and 30 non-volatile compounds of different classes of phytochemicals including phenolics, flavonoids, alcohols and aldehydes, esters, monoterpenoids, diterpenoids, triterpenoids, sesquiterpenoids (Zheng et al., 2016; Amarasiri et al., 2018).

Therefore, the present work concentrated on the preparation of CQDs by microwave-assisted green synthesis method using the leaves of the Mexican Mint (*Plectranthus amboinicus*) plant as the raw materials. The physicochemical properties of CQDs, such as particle size, optical properties, surface functional groups, and elemental composition were characterized using various techniques. Subsequently, the synthesized CQDs were used as an effective "turn-off" fluorescent sensor for the detection of Fe^{3+} ions and studied their sensitivity and selectivity. Further, the fluorescence of the CQD-Fe^{3+} system was recovered using ascorbic acid. With this fluorescent turn ON-OFF behaviour, NOT and IMPLICATION logic gate operations were performed. Finally, the cytotoxicity of CQDs was tested by the MTT assay using MCF-7 cells as a model cell for bioimaging applications.

2. Materials and methods

2.1. Chemicals

All chemicals were of analytical grade and were used without any further purification. $FeCl_3$, $BaCl_2$, $MnCl_2$, $PbCl_2$, $CuCl_2$, $BiNO_3$, $ZnCl_2$, $NiCl_2$ were purchased from HiMedia, India. *Plectranthus amboinicus* leaves were collected from the Bharathiar University Campus, Coimbatore (11.0398° N, 76.8790° E). The collected leaves were washed thoroughly and dried before use. Deionized water (DI) was used throughout all the experiments.

2.2. Synthesis of CQD from Mexican Mint by microwave-assisted reflux method

The Carbon quantum dots were prepared from the fresh leaves of Mexican Mint via the microwave-assisted reflux method. The collected leaves were cleaned thoroughly and washed using DD water. The rinsed leaves (50 gm) were ground with 50 mL of DD water using a mortar and pestle and collected the leaf extract. Then the desired amount of leaf extract is irradiated (4, 5, 6, and 7 min) with 80% power of the total 1200 W power under the domestic LG microwave oven. The irradiated sample was collected and centrifuged at 5000 rpm for 20 min. The supernatant solution was collected and purified using the column chromatography technique (Cheng et al., 2019). The purified sample was kept in a vacuum oven for 24 h for drying. The dried powder sample was used for further characterization studies. Scheme 1 represents the synthesis procedure of CQD preparation from the leaves of Plectranthus *amboinicus*.

2.3. Characterization

Carbon quantum dots synthesized from Mexican Mint leaves were characterized via different techniques. The XRD pattern was recorded using a Malvern Panalytical instrument with Cu-Ka radiation of wavelength 1.5406 Å. The morphology of biomass-derived CQD was analysed using TEM images through JEOL JEM 2100 High-resolution transmission electron microscope. The chemical composition of CQD was studied using XPS through Thermo scientific Multi-lab 2000 system. UV–vis absorption spectra were recorded using Varian Cary 5000 UV–vis spectrophotometer, and the photoluminescence spectra were recorded using Fluoromax Plus Spectrofluorimeter. Fourier transform infrared spectroscopy (FTIR) measurements were performed using a JASCO FT-IR – 6600 instrument.

2.4. Fe^{3+} sensing analysis

For the sensing analysis, various metal ions including Fe, Pb, Mn, Ni, Cu, Bi, Ba and Zn were tested for their presence in the drinking water. Each metal was taken at 15 μM concentration and mixed with 1 mL of

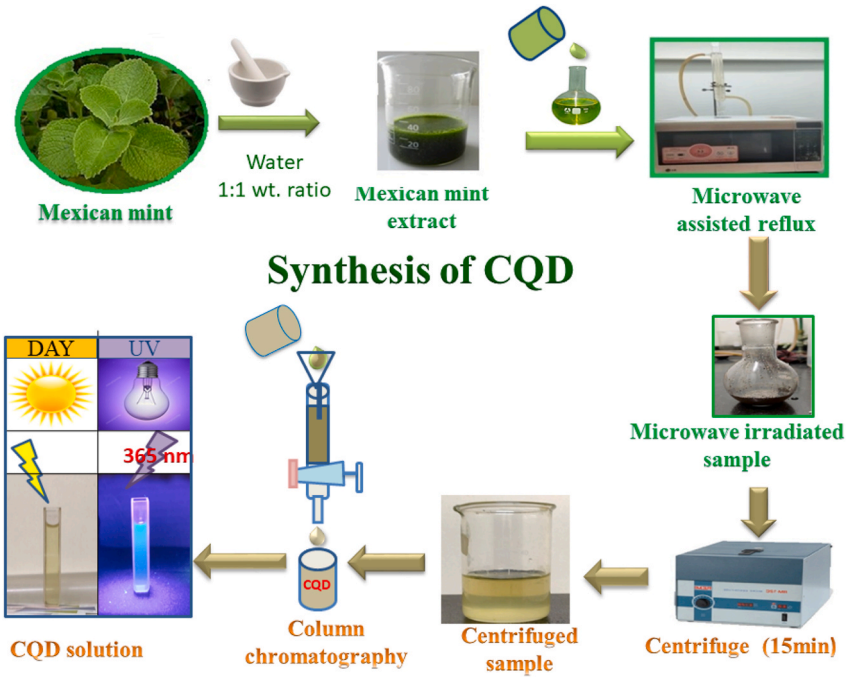

Scheme 1. Synthesis procedure of CQD derived from Mexican mint.

water. Then 2 mL of CQD solution was added dropwise to the metal stock solution and was stirred for 15 min using a magnetic stirrer. Interestingly, the metal ion solution containing iron showed a colour change from yellow to black. Thus the CQD solution was sensitive to the iron metal ions, with this sensing property the fluorescence emission and other characteristics were studied.

2.5. Fluorescent ink

The aqueous solution of CQD synthesized from *Plectranthus amboinicus* leaves was conveniently utilized as a fluorescent ink for writing letters and drawing patterns (coding) based on their excellent dispersibility, stability, and strong fluorescence capacity. For the preparation of fluorescent ink, the thin film was developed by mixing PVA and CQDs solution in the ratio of 1:10 and stirred well. Subsequently, the PVA and CQD mixture was drop-casted in a Petri dish and maintained at 45-degree Celsius for 2 h. The formed thin film layer of CQDs was peeled off and used further.

2.6. MTT assay and bio-imaging studies

To extend the biological application of the prepared CQDs, the cell cytotoxicity was tested via MTT assay using MCF-7 cells. Human breast cancer cells (MCF-7) were cultured in Dulbecco's modified Eagle's medium (DMEM) under the condition of 5% CO_2 and 37 °C. The cells were seeded into 96-well plates and allowed to adhere for 24 h. Then the different concentrations (0, 25, 50, 75, 100 μg/mL) of purified CQDs by dialysis were added to each well and maintained for another 24 h. Afterwards, the medium with diluted CQDs was discarded and the cells were washed using PBS solution 3 times. MTT solution was added to each well in all plates and incubated for another 4 h. Subsequently, the medium was carefully removed and DMSO (100 mL) was added to dissolve the formazan crystals. The absorbance was recorded at 595 nm using a microtitre plate reader (Bio-Rad, USA). For imaging studies, the CQDs (100 μg/mL) was allowed to stand for 2 h. Later, the media containing CQDs were removed and the cells were washed with phosphate buffer saline (PBS) twice. Finally, a fluorescence microscope (Accuscope EI 310, USA) was used to record images using a blue filter. The cell viability was calculated using equation (1),

$$\text{Cell viability } (\%) = \left(A_{\text{Sample}} / A_{\text{Control}}\right) \times 100 \quad (1)$$

Where,

A_{Sample} is the absorbance in the presence of CQD,

$A_{Control}$ is the absorbance in the absence of CQD.

3. Results and discussion

3.1. Structural, optical and morphological properties of CQDs

The formation of carbon quantum dots from the Mexican Mint leaves is revealed with the help of UV–vis absorption spectroscopy. Fig. 1 shows the UV–vis spectra of CQDs prepared at different microwave

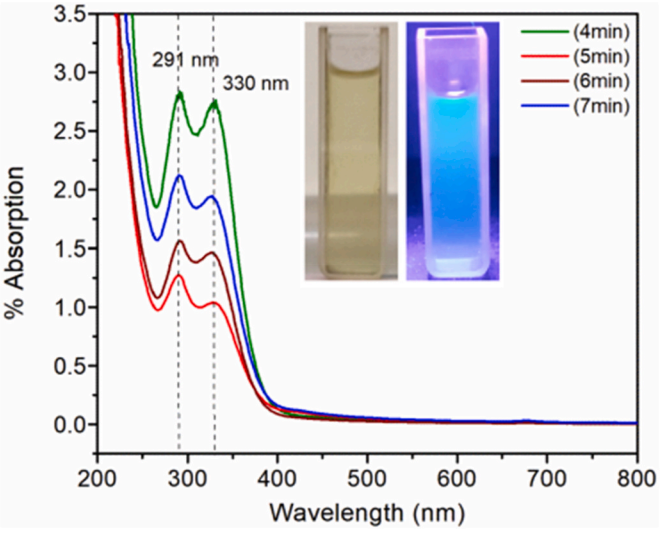

Fig. 1. UV–Vis spectra of Carbon quantum dots prepared from Mexican Mint by microwave irradiation and the inset shows the CQD solutions under Normal light and UV light.

irradiation times of 4, 5, 6, and 7 min. It can be seen that two strong absorption peaks observed at 291 nm and 330 nm for all the samples corresponding to the transitions of π-π* of C═C and n-π* of C═O functional groups (Melhuish et al., 1960; Zhan et al., 2019; Huang et al., 2019). Typically, the π-π* transition is due to the aromatic sp^2 domains in the carbon core, and n-π* transition is due to the carboxyl groups on the surface of the fluorescent Carbon dot (Yue et al., 2019; Shi et al., 2019). Among the samples prepared at different periods, the maximum absorption was obtained for the CQD prepared at 4 min. Hence, it is used for further studies, as it showed the most substantial absorption peak. The inset images show the prepared CQDs exposed under both sunlight and UV light.

In the photoluminescence spectroscopy, the CQD samples are excited at different wavelengths from 320 nm to 440 nm, and the fluorescence properties are studied. Fig. 2a shows the PL emission spectra of the CQD prepared from biomass at the different excitation wavelengths. Initially, the CQDs are excited from a wavelength of 260 nm to 300 nm, but no prominent emission peak was observed. On the other hand, while using the excitation wavelength from 320 to 380 nm, a sharp emission peak centred at 436 nm was observed. However, the maximum intensity was obtained at the low excitation wavelength of 340 nm due to the $n- \pi^*$ transition. While further increasing the excitation wavelength from 400 to 440 nm, the emission wavelength shifted from the blue to the red region (420–480 nm). This excitation dependent emission property is mainly dependent upon various parameters including surface states of C═O bonds (Sciortino et al., 2016), polydispersity and surface heterogeneity (Liu et al., 2017a, 2017b), etc. In the present case the presence of C═O bonds and the polydispersity was observed through FTIR and HRTEM analysis, respectively. As well as, while transmitting the electrons from non-bonding orbitals to bonding orbitals with smaller energy i.e. at higher excitation wavelengths, the wavelength of emission spectra tends to increase. Besides, the solvent polarity also induces the emission wavelength from the blue to the red region (Gharat et al., 2019). A similar type of blue-emitting carbon dots (CDs) was obtained from a milk protein and their interaction with *Spinacia oleracea* leaf cells (Bajpai et al., 2019). Huang et al. (2018) prepared CQD from Bauhinia flower and reported the maximum emission wavelength located at 442 nm with the corresponding optimal excitation wavelength at 355 nm. CQD prepared from the black soya beans by Jia et al. (2019) showed a PL peak at 470 nm with excitation of 360 nm. Shen et al. (2017) prepared the CQDs from sweet potato and obtained the PL. emission peak at 442 nm which is nearly equal to the present work. Similarly, they have reported that the PL emission peaks were red-shifted from 406 to 486 nm while varying the excitation wavelength from 300 nm to 410 nm.

The representative XRD pattern of CQDs prepared at 4 min is given in Fig. 2b. The observed sharp peaks at 28.28°, 40.46° and 50.12° corresponding to the (002), (100) and (102) planes of graphitic carbon of sp^2 hybridization (Naik et al., 2020). The peaks at 58.66° and 66.31° correspond to the planes of (600) and (220) of the diamond carbon structure of sp^3 hybridization (Souza et al., 2018). The obtained results are well-matched with the CD synthesized from the biomass of coconut husk by Chunduri et al. (2016), coffee grounds by Hsu et al. (2012) and coconut coir by Chauhan et al. (2020).

The FTIR spectrum of biomass-derived CQD is shown in Fig. 2c. It is well known that the surface of the CQD contains abundant different organic compounds such as –OH, C–H, C═O, C═C and C–O depend upon the raw materials. The spectrum infers that the peak observed at 3276 cm^{-1} corresponds to the stretching vibration of the O–H group present at the surface of the CQD. The presence of stretching C–H group confirmed by the band appeared at 2874 cm^{-1}. The observed band at

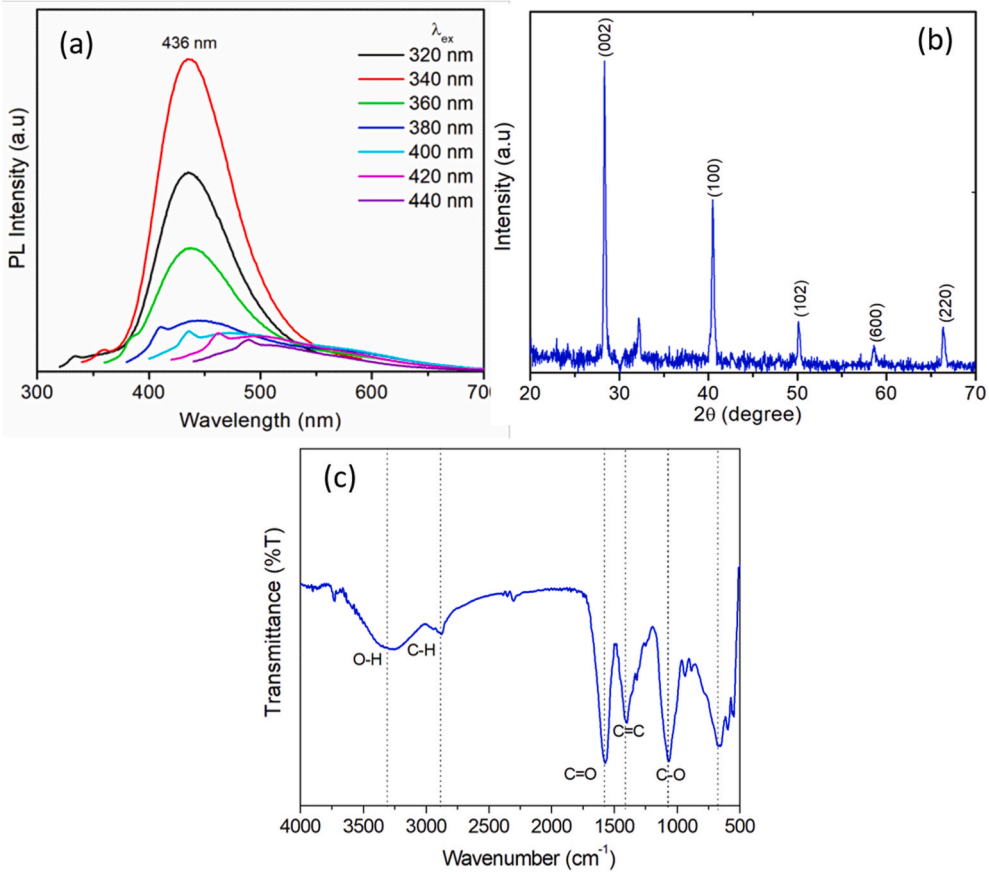

Fig. 2. (a) The PL emission spectra of CQDs prepared from biomass at various excitation wavelengths, (b) XRD pattern and (c) FTIR spectrum of CQDs prepared from biomass by microwave irradiation method.

1581 cm^{-1} corresponding to the occurrence of the C═O group. The C═C group appeared at 1406 cm^{-1}, and the peak at 1066 cm^{-1} corresponds to the bending vibration of the C–O group. The observed two peaks in the fingerprint region, i.e., 934 cm^{-1} and 661 cm^{-1} is due to the aromatic sp^2 bending. Similar results were obtained by Roy et al. (2014) who prepared the CQD from the fenugreek leaves they have observed the stretching of C═O at 1586 cm^{-1} and the bending of C–H at 1420 cm^{-1}. Lu et al. (2018) have also obtained similar results for the CQD prepared from watermelon juice with peaks at 2854 cm^{-1} and 1056 cm^{-1} corresponding to the C–H stretching and C–O groups on the surface of the CQDs. The CQD prepared from the coconut coir by Chauhan et al. (2020) showed similar peaks at 2960 cm^{-1} and 1450 cm^{-1} corresponding to the C–H stretching and CH_2 bending and one peak in the fingerprint region at 650 cm^{-1} correspondings to the aromatic sp^2 bending.

Further, X-ray photoelectron spectroscopy was used to examine the chemical composition and structure of carbon quantum dots. Fig. 3 shows the deconvoluted XPS spectra of the CQD sample synthesized from the leaves of *Plectranthus amboinicus*. The two strong binding energy peaks at 284.7 eV and 531.8 eV, attributing to C1s and O1s respectively (Chen et al., 2019; Wan et al., 2019). Fig. 3a depicts the high-resolution peaks of C1s. The C1s spectrum is resolved into three peaks at 284.6eV which is due to the C═C, the other two peaks at 285.9 eV and 288.5eV that attributes to the C–O and C═O bonds, respectively. Fig. 3b shows the high-resolution peaks of O1s. The O1s XPS spectrum of the CQDs is de-convoluted, the binding energies at 530.6 eV, 531.7 eV and 532.9eV ascribed to the HO–C═O, C–O and C–OH bands, respectively (Singh et al., 2019; Jayaweera et al., 2019; Atchudan et al., 2018).

The UV–vis absorption spectra and PL emission spectra of CQD and quinine sulfate solutions are measured to calculate the quantum yield and are given in Fig. 4 (a, b). Equation (2) is used to calculate the quantum yield, where the quinine sulfate, 5×10^{-3} M in 1 N H_2SO_4 with quantum yield, $\phi_{std} = 54\%$ was used as the reference (Melhuish, 1960).

$$QY = \varphi_{std}\frac{I_{sample}}{I_{std}}\frac{A_{std}}{A_{sample}}\frac{\eta^2_{std}}{\eta^2_{sample}} \tag{2}$$

where,

QY *and* φ_{std}, are the fluorescence quantum yield of the CQD and the standard quinine sulfate.

I_{sample} *and* I_{std} are the integrated fluorescence intensity of CQD and the standard quinine sulfate.

A_{sample} *and* A_{std} are the absorbance values of CQD and the standard quinine sulfate,

η_{sample} *and* η_{std} are the refractive indices of the sample and standard.

A series of CQD solutions and quinine sulfate were prepared and the absorption was kept less than 0.1 to reduce the inner filter effects (Schneider et al., 2019) and the obtained above parameters are given in Table 1. A quantum yield of 17% was obtained for the CQD derived from the Mexican Mint leaves (Feng et al., 2016).

The morphology and particle size of Carbon quantum dots prepared from the Mexican Mint leaves were characterized using TEM analysis, as the photoluminescence (PL) properties of CQDs are mostly dependent on particle size. Fig. 5a, b shows that the prepared carbon quantum dots are spherical in size having less than 5 nm. The individual particles are dispersed uniformly without any agglomeration. The calculated lattice spacing, 0.222 nm is corresponding to the lattice plane of (100) plane. However, in addition to the monodispersed CQDs (Fig. 5 a, b), the aggregated and well defined highly crystalline CQDs also observed (Fig. 5c). The measured interplanar spacings of 0.222 nm and 0.3118 nm correspond to the lattice planes of (100) and (002), respectively. The particle size histogram (Fig. 5d) indicates that the size of the particles lying in between 0.5 and 5 nm and the maximum number of particles having a size range of 2.43 ± 0.02 nm. The SAED pattern (Fig. 5c inset) reveals the crystalline nature of CQD, which is in agreement with the X-ray diffraction results.

3.2. Metal ion sensing applications

Though numerous analytical techniques available for identifying the level of metals, an easy and cost-effective way is to make use of the CQD as the sensing probe. Fig. 6a shows the PL spectra of blank CQD and with different metals ions (Mn^{2+}, Fe^{3+}, Ni^{2+}, Cu^{2+}, Zn^{2+}, Ba^{2+}, Pb^{2+}, Bi^{3+}) to study the fluorescence quenching properties. It can be seen that the empty or the blank CQD solution has a maximum emission intensity at 447 nm, and with the addition of different metal ions, the fluorescence intensity gets diminished. On the addition of different metal ions, the quenching of fluorescence was observed, thereby the emission intensity started to decrease. The quenching constant of different metal ions was calculated using the Stern-Volmer formula (eqn. (3)), and it was inferred that the maximum quenching was observed on the addition of Fe^{3+} ions to the CQD solution (Fig. 6b).

$$\frac{F}{F_o} = 1 + K_{SV}(Q) \tag{3}$$

where.

F_0 – fluorescence intensity of the standard CQD solution.

F - fluorescence intensity of metal ion solution.

K_{SV} - Stern Volmer quenching constant.

The quenching decreased in the order of Fe^{3+}, Mn^{2+}, Cu^{2+}, Zn^{2+}, Pb^{2+}, Ba^{2+}, Bi^{3+} and Ni^{2+} and the lowest quenching was observed for the Ni^{2+} ions. The higher selectivity of Fe^{3+} is due to the ion-selective nature of functional groups present on the surface of CQD and their charge selective nature. The oxygen groups present on the surface of CQD interact with the Fe^{3+} and lead to the formation of complexes.

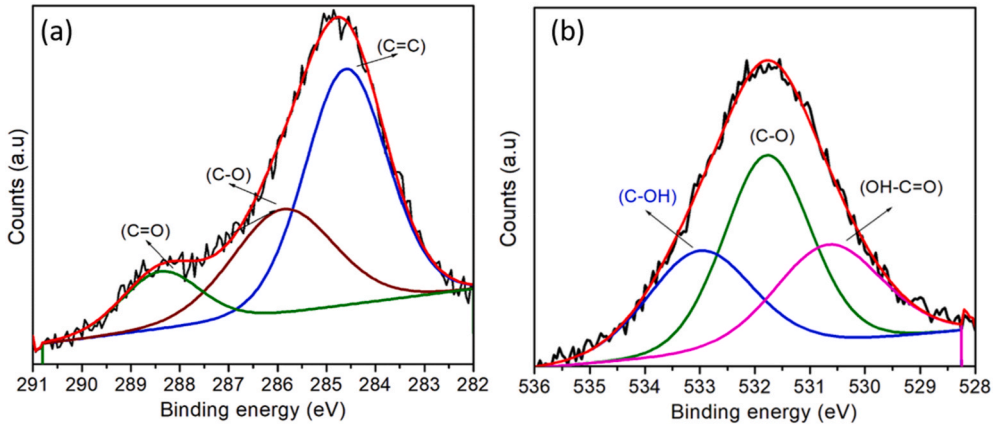

Fig. 3. The deconvoluted XPS spectra (a) C 1s and (b) O 1s peaks.

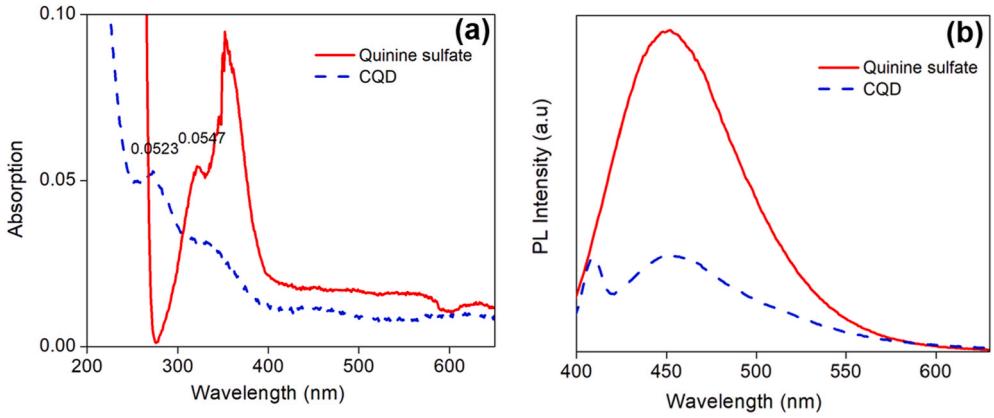

Fig. 4. (a) UV–vis absorption spectra and (b) PL emission spectra of CQD and quinine sulfate.

Table 1
Data for calculating the fluorescence quantum yield of CQD.

Sample	Absorbance (A) (at 350 nm)	Integrated area (I) (400–630 nm)	Refractive index (η)	Quantum yield
Quinine sulfate (Std)	0.0547	1.19349×10^8	1.33	0.54
CQD	0.0523	3.6687×10^7	1.33	0.17

These complexes affect the distribution of surface energy traps and enhance the non-radiative recombination of electrons and holes which causes fluorescence quenching (Das et al., 2019).

The sensitivity of CQDs for the detection of Fe^{3+} ions was estimated with the relationship between the fluorescence quenching of CQDs and the different concentrations of Fe^{3+} ions from 0 μM–15 μM (0, 5, 10, and 15 μM). Fig. 6c shows the Fluorescence spectra of CQDs in the presence of a different concentration of Fe^{3+} and the inset of Fig. 6c shows the linear relationship between F_0/F and the concentration of Fe^{3+} ions. It is seen that the fluorescence intensity of CQD decreases gradually with increasing the concentration of Fe^{3+} ions in the order of 0, 5, 10 and 15 μM. The PL spectra depict that the decrease in fluorescence intensity on the increase in the concentration of Fe^{3+} ions. The mechanism of fluorescence quenching of CQDs in the presence of Fe^{3+} ion is caused by the electron transfer between CQDs and Fe^{3+}ions. A good linear relation (Regression equation: $y = 0.5529x + 0.00981$, $R^2 = 0.9111$) is observed over the concentration range of 0–15 μM. The limit of detection (LOD) was calculated using equation (4).

$$Limit\ of\ detection = \frac{3\sigma}{s} \tag{4}$$

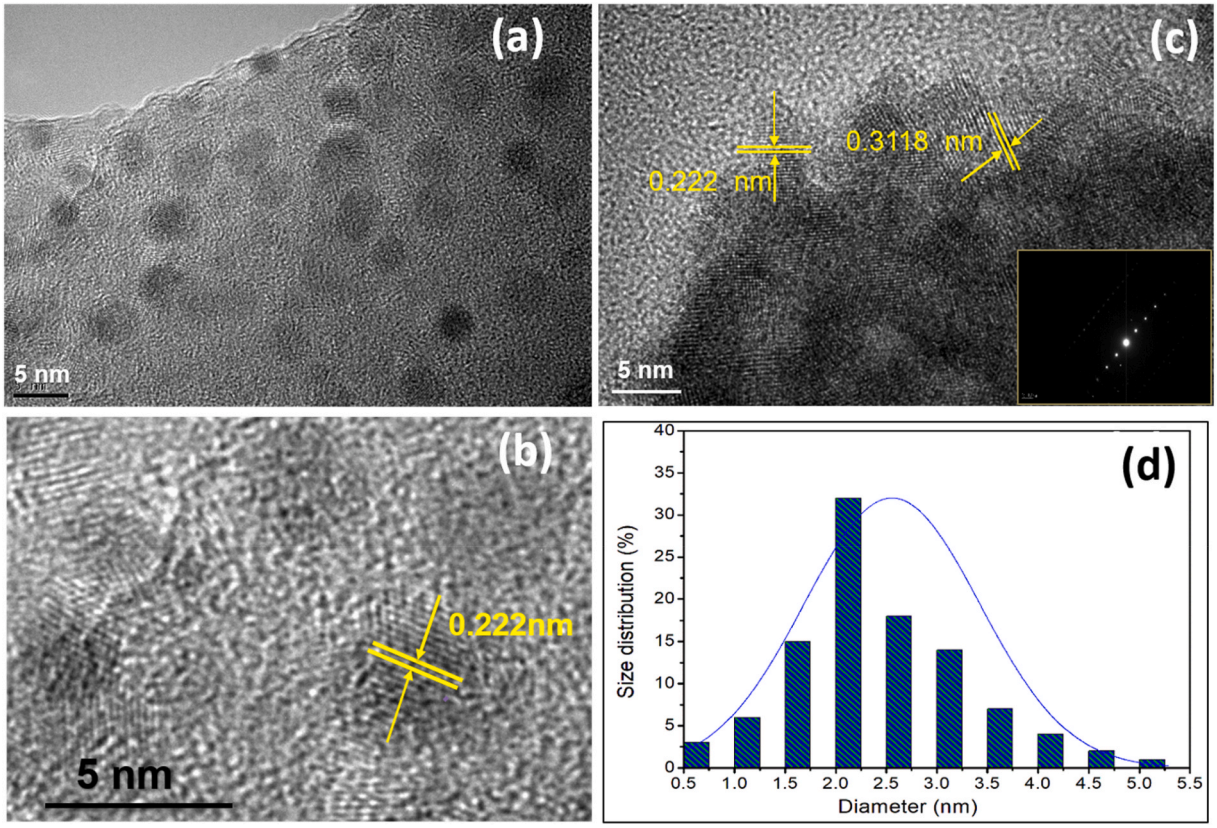

Fig. 5. (a–c) HRTEM images and (d) the particle size histogram of prepared CQDs particles (inset: Corresponding SAED pattern).

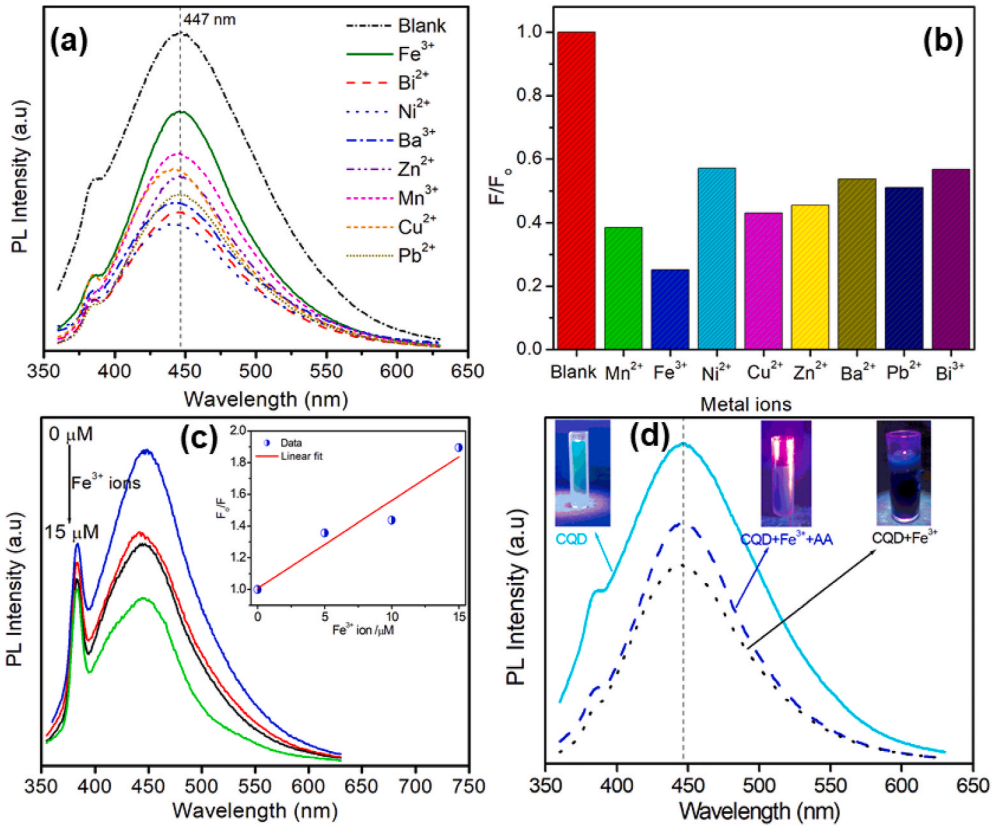

Fig. 6. (a) The PL spectra of blank CQD and the presence of different metal ions, (b) The difference in relative PL intensities of CQD between the blank and solutions containing different metal ions, (c) Fluorescence spectra of CQDs in the presence of a diverse concentration of Fe^{3+} ions, inset shows the linear relationship between F_0/F and the concentration of Fe^{3+} in the range of 0–15 μM and (d) The PL Spectra of fluorescence quenching and re-quenching properties.

where.

σ is the value of standard deviation and

s is the slope of the linear fit (Raveendran et al., 2019).

The calculated LOD is 0.53 μM for the prepared CQDs, which is comparable with the previous literature (Table 2).

Fig. 6d shows the quenching and re-quenching behaviour of CQDs. For the re-quenching of fluorescence of CQD, 15 μM of Ascorbic Acid (AA) was added to the above solution. Interestingly, the colour of the CQD solution changes from black to yellow, which infers that the fluorescence property was regained. As Fe^{3+} and AA have a high binding affinity, the restoration of fluorescence is attributed to the release of loosely bound Fe^{3+} from the surface of CQD. With the fluorescence quenching and re-quenching mechanism, the turn ON-OFF assay was performed, and the logic gate operation was also studied. Scheme 2 depicts the schematic representation of the fluorescence ON- OFF assay of the biomass-derived carbon dots.

Table 2
Comparison of CQDs derived from various biomass for Fe^{3+} sensing.

Precursor	Linear range	Limit of detection	Reference
Lychee	0.1–1.6 μM	23.6 nm	Sahoo et al. (2019)
Rose heart radish	0.02–40 μM	0.13 μM	Liu et al. (2017a, 2017b)
Mint leaf	0–0.38 μM	0.37 μM	Raveendran et al. (2019)
Hydrogenated rosin	0–60 μM	6.16 μM	Zhou et al. (2020)
Miscanthus grass	0–100 μM	0.02 μM	Picard et al. (2019)
Lycii Fructus	0–30 μM	21 nM	Sun et al. (2017)
Rice residue and glycine	3.32–32.26 μM	0.7462 μM	Qi et al. (2019)
Phyllanthus acidus	2–25 μM	0.9 μM	Atchudan et al. (2018)
Willow catkin	40–700 μM	0.03 μM	Cheng et al. (2019)
Black soya beans	0.2–300 μM	96.87 nm	Jia et al. (2019)
Mexican Mint	0–15 μM	0.53 μM	Present work

Logic gates are simple logic circuits that may be fed with one or more input values to give the desired output values depending upon the operations to be performed. Here the fluorescence quenching property of the CQD solution on the addition of Fe^{3+} ions and the fluorescence re-quenching property on further addition of AA is taken. The quenching re-quenching property of the CQD at different input conditions is checked with the help of the NOT and the IMPLICATION logic gates (Bandi et al., 2018). A NOT gate is also called an inverter, or the not gate is a logic gate that implements logical negation. Each NOT gate has only one input signal. Logically with NOT gates, the input and the output swap, so if the input is 1, then the output is 0 and vice versa. With this basic knowledge, the NOT gate was constructed, and the performance was studied. Fig. 7a represents the NOT logic gate and its truth table. Here the NOT gate operation was performed based on the fluorescence quenching of the CQD. The presence of Fe^{3+} was considered as input 1, and the absence of Fe^{3+} as 0 input. In the absence of Fe^{3+}, the CQD solution showed maximum intensity, and this state has an output of 1 (ON state), the presence of Fe^{3+} the CQD solution showed no intensity, and this output is taken as 0 (OFF state). With this information, the logic gate and the truth table was drawn.

The IMPLY gate is a digital logic gate that implements a logical relation between two propositions. The implication logic gate consists of two inputs, of which one is directly connected to one of the inputs of an OR gate. The other input is fed into a NOT gate; the inverted output from the NOT gate is fed as the second input of the OR gate. The output of the OR gate is taken as the final output of the IMPLY gate. With this basic knowledge, the implication logic gate was constructed, and the performance was studied. Fig. 7b represents the IMPLICATION logic gate and

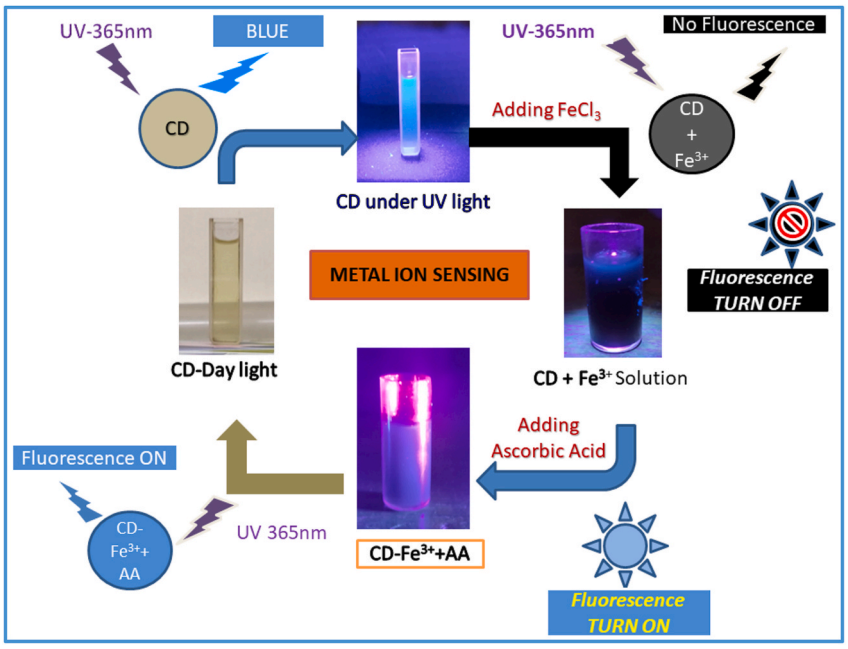

Scheme 2. The schematic representation of fluorescence turn ON-OFF assay of biomass-derived CQD.

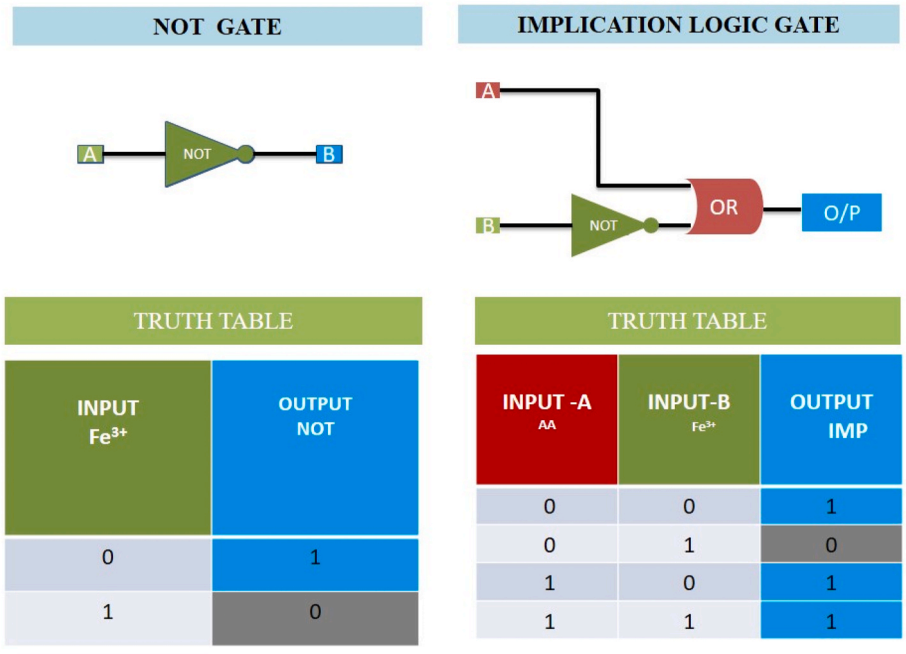

TRUTH TABLE

INPUT Fe^{3+}	OUTPUT NOT
0	1
1	0

TRUTH TABLE

INPUT -A AA	INPUT-B Fe^{3+}	OUTPUT IMP
0	0	1
0	1	0
1	0	1
1	1	1

Fig. 7. NOT and IMPLICATION logic gates and their Truth tables.

its corresponding truth table. Based on the Fe^{3+} and AA-sensitive switching system, an IMPLICATION logic gate was designed. The presence of Fe^{3+} and AA were considered to be the input "1" state, and the absence of Fe^{3+} and AA was as "0" state. Four different input conditions were fed, and the corresponding output was noted. It was seen that with the absence of both Fe^{3+} and AA (0/0) state maximum fluorescence was seen and the output is taken as 1 (ON state). In the absence of AA and the presence of Fe^{3+} (0/1) as the input condition, there was no fluorescence, and the output is 0 (OFF state). With the presence of only AA and absence of Fe^{3+}, i.e., (1/0) as the input state, the CQD solution showed fluorescence and the output is 1(ON state). With the presence of both the AA and Fe^{3+} ((1/1 state) the fluorescence was seen, and the output is 1 (ON state). Hence, the prepared CQDs can be used to design the next generation molecular logic devices.

3.3. Fluorescent ink properties

Green synthesis biomass CQD's possess the most attractive optical properties such as good photostability and excellent fluorescent property. It can be used as fluorescent ink for coding and decoding secret information (Atchudan et al., 2018). since it is easy to prepare, eco-friendly and cost-effective. The aqueous solution of CQD synthesized from *Plectranthus amboinicus* leaves was conveniently utilized as a fluorescent ink for writing letters and drawing patterns (coding) based

on their excellent dispersibility, stability, and strong fluorescence capacity. The photographic optical images of an aqueous dispersion of CQDs in both daylight and UV light (365 nm) exposure are depicted in Fig. 8. Fig. 8 (a and b) shows the handwritten letters of the Tamil language using the synthesized CQD and their fluorescent behaviour. The comic character, iron man heart was drawn using fluorescent ink on the black surface and its blue fluorescent under the irradiation of UV light is shown in Fig. 8 (c and d). Further, the PVA and CQDs were mixed in a 1:10 ratio as a solution and drop-casted on a Petri dish and dried using the hot-air oven for 2hr at 45 °C. Subsequently, the formed thin film layer of CQDs was peeled off and exposed to sunlight and UV light (Fig. 8e and f), where the bright blue emission was seen.

3.4. Biological properties

3.4.1. Cytotoxicity and cell imaging

As explained previously, the *Plectranthus amboinicus* (Mexican Mint) leaves have been used for a wide range of pharmaceutical applications that included antimicrobial, antiinflammatory, antitumor, wound healing, anti-epileptic, larvicidal, antioxidant, and analgesic activities (Arumugam et al., 2016). As well, these leaf extracts were used in the preparation of metallic nanoparticles of silver (Ajitha et al., 2014), gold (Purusottam Reddy et al., 2017), etc. However, experiments about *Plectranthus amboinicus* for the synthesis of CQDs are scarce with biological significance. Hence, the present study aims to estimate the cytotoxicity of CQDs using MTT assay through the viabilities of MCF7 Breast cancer cells. Fig. 9 shows the cell viabilities of CQDs prepared under different microwave irradiation time (4, 5, 6 and 7 min) with different concentrations (0, 25, 50, 75, 100 μg/mL). Among these, the sample irradiated for 4min shows about 80% cell viability at 20 μg/mL concentration and almost constant viability at even higher concentrations. Thus the CQD synthesized from the Mexican Mint leaves are highly biocompatible and show low cytotoxicity. Therefore, the

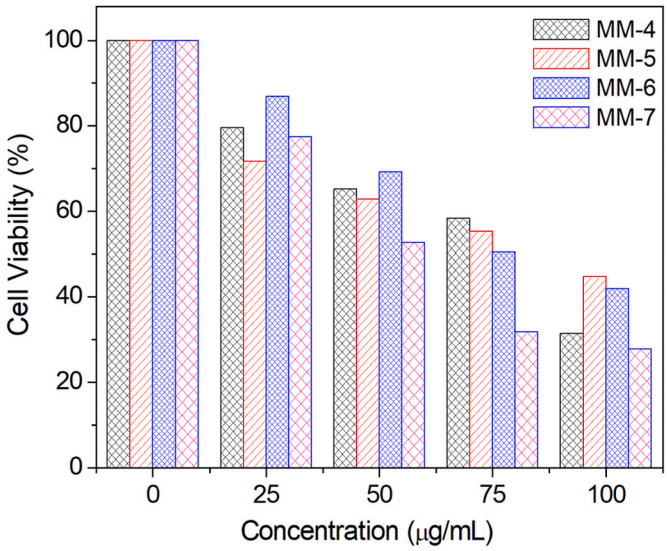

Fig. 9. MTT assay of CQDs in MCF-7 human breast cancer cell line.

prepared CQDs can be effectively used in live-cell imaging as biomarkers. Fig. 10 (a,b) shows the fluorescence images of MCF 7 breast cancer cells incubated with CQDs (100 μg/mL) under a bright field. The cells emitted strong blue fluorescence when excited at 360 nm. However, no emission was obtained in the control sample. Arumugham et al. (2020) has prepared the CQDs from *Catharanthus roseus,* which shows the 82% cell viability and obtained the clear penetration at 500 μL/mg for MCF7 breast cancer cell imaging. Similarly, *Andrographis paniculata* leaves derived pink colour fluorescent CQDs exhibits 50% cell viability and slightly good permeability for the cell imaging reported by Naik et al. (2020). Comparatively, the prepared CQDs from Mexican Mint

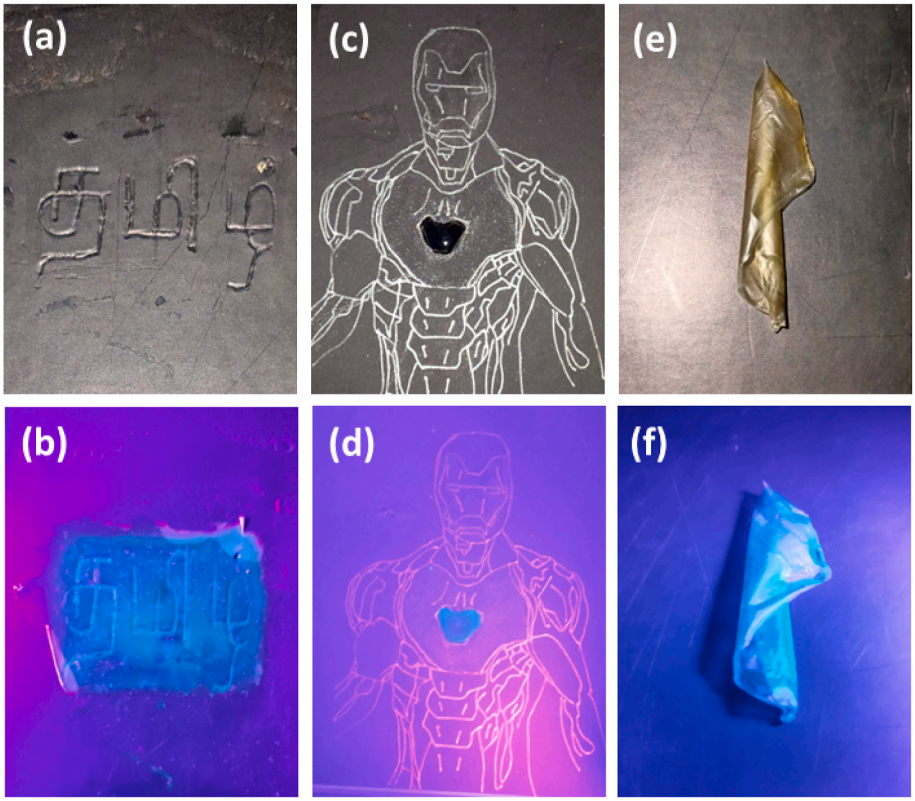

Fig. 8. Photographic image of (a, b) hand -written Tamil words, **(c, d)** hand-drawn comic character iron man heart and (e, f) CQD-PVA film exposed under normal light and UV irradiation.

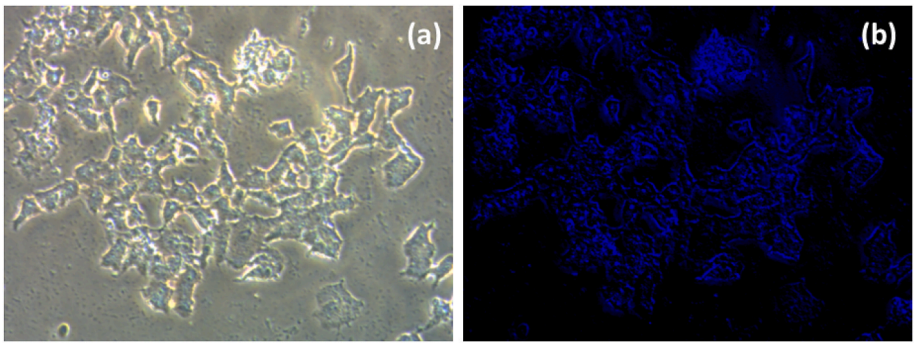

Fig. 10. Fluorescence images of MCF 7 breast cancer cells incubated with CQDs (100 μg/mL) (a) under bright field, (b) under 360 nm excitation.

shows better performance in terms of cell viability and bio-imaging due to the good permeability and biocompatibilities. Overall, the observed distinctive blue emission infers that the prepared CQDs can be used as optical nanoprobes for bio-imaging applications.

4. Conclusions

In summary, blue-emitting carbon quantum dots were successfully synthesized from the *Plectranthus amboinicus* (Mexican Mint) leaves via the Microwave-assisted reflux method. The CQD were spherical with an average diameter of about 2.43 ± 0.02 nm. Besides, the characterization of CQD showed that they have oxygen-containing functional groups on their surface which are beneficial in improvising the water solubility and fluorescence. The obtained CQD showed a fluorescence quantum yield of 17%. The CQDs were used as the fluorescent probe for Fe^{3+} ion detection. The CQDs were selectively quenched by Fe^{3+} ion and exhibited marvellous selectivity. It showed a good linear relationship ($R^2 = 0.9111$) with the limit of detection of 0.53 μM in the concentration range of 0–15 μM. With the fluorescent turn ON-OFF behaviour of CQD on the addition of Ascorbic Acid, the NOT and IMPLICATION logic gates were constructed and studied. Further, the fluorescent ink was prepared for writing letters and drawing patterns towards the coding and decoding process. Finally, the cytotoxicity and bio-imaging applications of the prepared CQDs were studied, which showed 80% of cell viability as well as better permeability for cell imaging at 100 μL/mg. Overall, the CQDs prepared at 4 min shows the excellent properties in terms of detection of Fe^{3+} ions and biological applications.

Credit author statement

Natarajan Architha, Formal analysis; Investigation; Writing – original draft. Murugesan Ragupathi, Formal analysis; Investigation; Writing – original draft. Chellappan Shobana, Investigation; Methodology; Writing – review & editing. Thangasamy Selvankumar, Resources; Writing – review & editing. Ponnuchamy Kumar, Resources; Writing – review & editing. Yun Sung Lee, Resources. Ramakrishnan Kalai Selvan, Conceptualization, Supervision; Writing – review & editing

Declaration of competing interest

The authors declare that they have no known competing financial interests or personal relationships that could have appeared to influence the work reported in this paper.

Acknowledgment

Prof. Yun Sung Lee acknowledges the Ministry of Science, ICT and Future Planning of South Korea for providing a National Research Foundation of Korea (NRF) grant (No. 2019R1A4A2001527).

References

Ajitha, B., Reddy, Y.A.K., Reddy, P.S., 2014. Biosynthesis of silver nanoparticles using *Plectranthus amboinicus* leaf extract and its antimicrobial activity. Spectrochim. Acta Mol. Biomol. Spectrosc. 128, 257–262.

Amarasiri, A.M.S.S., Attanayake, A.P., Jayatilaka, K., Mudduwa, L.K.B., 2018. Acute nephroprotective and antioxidant activities of aqueous leaf extract of Plectranthus amboinicus (Roxb.) grown in Sri Lanka. J. Pharmacogn. Phytochem. 7, 155–161.

Arumugam, G., Mallappa, K.S., Sinniah, U.R., 2016. Plectranthus amboinicus (lour.) Spreng: botanical, phytochemical, pharmacological and nutritional significance. Molecules 21, 369.

Arumugham, T., Alagumuthu, M., Amimodu, R.G., Munusamy, S., Iyer, S.K., 2020. A sustainable synthesis of green carbon quantum dot (CQD) from *Catharanthus roseus* (white flowering plant) leaves and investigation of its dual fluorescence responsive behavior in multi-ion detection and biological applications. Sustain. Mater. Technol. 23, e00138.

Atchudan, R., Edison, T.N.J.I., Aseer, K.R., Perumal, S., Karthik, N., Lee, Y.R., 2018. Highly fluorescent nitrogen-doped carbon dots derived from Phyllanthus acidus utilized as fluorescent probe for label-free selective detection of $Fe3^{+}$ ions, live-cell imaging and fluorescent ink. Biosens. Bioelectron. 99, 303–311.

Bajpai, S.K., Souza, A.D., Suhail, B., 2019. Blue light-emitting carbon dots (CDs) from a milk protein and their interaction with *Spinacia oleracea* leaf cells. Int. Nano Lett. 9, 203–212.

Bandi, R., Devulapalli, N.P., Dadigala, R., Gangapuram, B.R., Guttena, V., 2018. Facile conversion of toxic cigarette butts to N,S-codoped carbon dots and their application in fluorescent film, security ink, bioimaging, sensing and logic gate operation. ACS Omega 3, 13454–13466.

Chauhan, P., Dogra, S., Chaudhary, S., Kumar, R., 2020. Usage of coconut coir for sustainable production of high-valued carbon dots with discriminatory sensing aptitude toward metal ions. Materials Today Chemistry 16, 100247.

Chen, X., Bai, J., Ma, Y., Yuan, G., Mei, J., Zhang, L., Ren, L., 2019. Multifunctional sensing applications of biocompatible N-doped carbon dots as pH and Fe^{3+} sensors. Microchem. J. 149, 103981.

Cheng, C., Xing, M., Wu, Q., 2019. Universal facile synthesis of nitrogen and sulfur co-doped carbon dots from cellulose-based biowaste for fluorescent detection of Fe^{3+} ions and intracellular bioimaging. Mater. Sci. Eng. C 99, 611–619.

Chunduri, A., Kurdekar, A., Patnaik, S., Vishnu Dev, B., Rattan, T.M., Kamisetti, V., 2016. Carbon quantum dots from coconut husk: evaluation for antioxidant and cytotoxic activity. Materials Focus 5, 55–61.

Das, G.S., Shim, J.P., Bhatnagar, A., Tripathi, K.M., Kim, TaeY., 2019. Biomass-derived carbon quantum dots for visible-light-induced photocatalysis and label-free detection of Fe(III) and ascorbic acid. Sci. Rep. 9, 15084.

Dehvari, K., Liu, K.L., Tseng, P.J., Gedda, G., Girma, W.M., Chang, J.Y., 2019. Sonochemical- assisted green synthesis of nitrogen-doped carbon dots from crab shell as targeted nanoprobes for cell imaging. Journal of the Taiwan Institute of Chemical Engineers 95, 495–503.

Duraimurugan, K., Harikrishnan, M., Madhavan, J., Siva, A., Jun Lee, S., Theerthagiri, J., Yong Choi, M., 2021. Anthracene-based fluorescent probe: Synthesis, characterization, aggregation - induced emission, mechanochromism, and sensing of nitroaromatics in aqueous media. Environ. Res. 194, 110741.

Fan, Z., Nie, Y., Wei, Y., Zhao, J., Liao, X., Zhang, J., 2019. Facile and large-scale synthesis of graphene quantum dots for selective targeting and imaging of cell nucleus and mitochondria. Mater. Sci. Eng. C 103, 109824.

Feng, X., Zhang, Y., 2019. A simple and green synthesis of carbon quantum dots from coke for white light-emitting devices. RSC Adv. 9, 33789–33793.

Feng, J., Wang, W.J., Hai, X., Yu, Y.L., Wang, J.H., 2016. Green preparation of nitrogen-doped carbon dots derived from silkworm chrysalis for cell imaging. J. Mater. Chem. B 387–393, 4.

Gharat, P.M., Chethodil, J.M., Srivastava, A.P., Praseetha, P.K., Pal, H., Sharmistha, D.C., 2019. An insight into the molecular and surface state photoluminescence of carbon dots revealed through solvent-induced modulations in their excitation wavelength dependent emission properties. Photochem. Photobiol. Sci. 110–119, 18.

Hong, D., Deng, X., Liang, J., Li, J., Tao, Y., Tan, K., 2019. One-step hydrothermal synthesis of down/up-conversion luminescence F-doped carbon quantum dots for label-free detection of Fe^{3+}. Microchem. J. 151, 104217.

Hsu, P.C., Shih, Z.Y., Lee, C.H., Chang, H.T., 2012. Synthesis and analytical applications of photo luminescent carbon nanodots. Green Chem. 14, 917.
Huang, Q., Li, Q., Chen, Y.F., Tong, L., Lin, X., Zhu, J., Tong, Q., 2018. High quantum yield nitrogen-doped carbon dots: green synthesis and application as "off-on" fluorescent sensors for the determination of Fe^{3+} and adenosine triphosphate in biological samples. Sensor. Actuator. B Chem. 276, 82–88.
Huang, P., Xu, S., Zhang, M., Zhong, W., Xiao, Z., Luo, Y., 2019. Modulation doping of absorbent cotton derived carbon dots for quantum dot-sensitized solar cells. Phys. Chem. 21, 26133.
Jayaweera, S., Yin, K., Ng, W.J., 2019. Nitrogen-Doped durian shell derived carbon dots for inner filter effect mediated sensing of tetracycline and fluorescent ink. J. Fluoresc. 29, 221–229.
Jia, J., Lin, B., Gao, Y., Jiao, Y., Li, L., Dong, C., Shuang, S., 2019. Highly luminescent N-doped Carbon dots from black soya beans for free radical scavenging, Fe^{3+} sensing and Cellular imaging. Spectrochim. Acta Mol. Biomol. Spectrosc. 211, 363–372.
Li, Y., Liu, F., Cai, J., Huang, X., Lin, L., Lin, Y., Yang, H., Li, S., 2019. Nitrogen and sulfur co- doped carbon dots synthesis via one-step hydrothermal carbonization of green alga and their multifunctional applications. Microchem. J. 147, 1038–1047.
Lim, H., Liu, Y., Kim, H.Y., Son, D.I., 2018. Facile synthesis and characterization of carbon quantum dots and photovoltaic applications. Thin Solid Films 660, 672–677.
Liu, T., Cui, Z., Zhou, J., Wang, Y., Zou, Z.G., 2017a. Synthesis of pyridinic-rich N, S Co-doped carbon quantum dots as effective enzyme mimics. Nanoscale Research Letters 12, 375.
Liu, W., Diao, H., Chang, H., Wang, H., Li, T., Wei, W., 2017b. Green synthesis of carbon dots from rose-heart radish and application for Fe^{3+} detection and cell imaging. Sensor. Actuator. B Chem. 241, 190–198.
Liu, L., Yu, X., Yi, Z., Chi, F., Wang, H., Yuan, Y., Li, D., Xu, K., Zhang, X., 2019. High efficiency solar cells tailored using biomass-converted graded carbon quantum dots. Nanoscale 11, 15083–15090.
Lu, M., Duan, Y., Song, Y., Tan, J., Zhou, L., 2018. Green preparation of versatile nitrogen-doped carbon quantum dots from watermelon juice for cell imaging, detection of Fe3+ ions and cysteine, and optical thermometry. J. Mol. Liq. 269, 766–774.
Melhuish, W.H., 1960. A standard fluorescence spectrum for calibrating spectro-flurophotometers. J. Phys. Chem. 64, 762–764.
Mittal, L.D., Jha, S., Basu, H., Singhal, R.K., Park, T.J., Kailasa, S.K., 2019. Acid oxidation of muskmelon fruit for the fabrication of carbon dots with specific emission colours for recognition of Hg^{2+} ions and cell imaging. ACS Omega 4, 19332–19340.
Murugan, N., Sundramoorthy, A.K., 2018. Green synthesis of fluorescent carbon dots from Borassus flabellifer flower for label-free highly selective and sensitive detection of Fe^{3+} ions. New J. Chem. 13297–13307, 42.
Naik, V., Zantye, P., Gunjal, D., Gore, A., Anbhule, P., Kowshik, M., Sheshanath, V., Bhosale, Kolekar, G., 2019. Nitrogen-Doped carbon dots via hydrothermal synthesis: naked eye fluorescent sensor for dopamine and used for multicolour cell imaging. ACS Appl. Bio Mater. 2, 2069–2077.
Naik, G.G., Alam, MdB., Pandey, V., Mohapatra, D., Dubey, P.K., Avanish, S., Sahu, A.N., 2020. Multi-FunctionalCarbon dots from an ayurvedic medicinal plant for cancer cell bio-imaging applications. ACS Appl. Bio Mater. 30, 407–418.
Naik, G.G., Alam, M.B., Pandey, V., Dubey, P.K., Parmar, A.S., Sahu, A.K., 2020. Pink fluorescent carbon dots derived from the phytomedicine for breast cancer cell imaging. Chemistry 5, 6954–6960.
Picard, M., Thakur, S., Mohanty, A.K., Misra, M., 2019. Miscanthus grass-derived carbon dots to selectively detect Fe^{3+} ions. RSC Adv. 9, 8628.
Purusottam Reddy, B., Mallikarjuna, K., Narasimha, G., Park, S.H., 2017. Plectranthus amboinicus-mediated silver, gold, and silver-gold nanoparticles: phyto-synthetic, catalytic, and antibacterial studies. Mater. Res. Express 4, 085010.
Qi, H., Teng, M., Liu, M., Liu, S., Li, J., Yu, H., Teng, C., Huang, Z., Liu, H., Shao, Q., Umar, A., Ding, T., Gao, Q., Guo, Z., 2019. Biomass-derived nitrogen-doped carbon quantum qots: highly selective fluorescent probe for detecting Fe^{3+} ions and tetracyclines. J. Colloid Interface Sci. 539, 332–341.
Qian, K., Guo, H., Chen, G., Ma, C., Xing, B., 2018. Distribution of different surface modified carbon dots in pumpkin seedlings. Sci. Rep. 8, 7991.
Ramu, A.G., Telmenbayar, L., Theerthagiri, J., Yang, D., Songa, M., Choi, D., 2020. Synthesis of a hierarchically structured Fe_3O_4–PEI nanocomposite for the highly sensitive electrochemical determination of bisphenol A in real samples. New J. Chem. 44, 18633–18645.
Raveendran, V., Rajukrishnan, A., Babu, S., Renuka, N.K., 2019. Mint leaf derived carbon dots for dual analyte detection of Fe(III) and ascorbic acid. RSC Adv. 9, 12070.
Roy, P., Periasamy, A.P., Chuang, C., Liou, Y.R., Chen, Y.F., Joly, J., Liang, C.T., Chang, H.T., 2014. Plant leaf-derived graphene quantum dots and applications for white LEDs. New J. Chem. 38, 4946–4951.
Sahoo, N.K., Jana, G.C., Aktara, M.N., Das, S., Nayim, S.K., Patra, A., Bhattacharjee, P., Bhadra, K., Hossain, M., 2019. Carbon dots derived from lychee waste: application for Fe^{3+} ions sensing in real water and multicolour cell imaging of skin melanoma cells. Mater. Sci. Eng. C 108, 110429.
Schneider, E.M., Bärtsch, A., Stark, W.J., Grass, R.N., 2019. Safe one-pot synthesis of fluorescent carbon quantum dots from lemon juice for a hands-on experience of nanotechnology. J. Chem. Educ. 96, 540–545.
Sciortino, A., Marino, E., Dam, B., Schall, P., Cannas, M., Messina, F., 2016. Solvatochromism unravels the emission mechanism of carbon nanodots. J. Phys. Chem. Lett. 7, 3419–3423.
Sedhu, N., Vasanthakumar, V., Theerthagiri, J., Ramachandran, A., Raj, V., 2020. Nickel hexa cyanoferrate film-coated pencil graphite electrode as sensor and electrode material for environment and energy applications. Int. J. Energy Res. 44, 10206–10221.
Shen, J., Shang, S., Chen, X., Wang, D., Cai, Y., 2017. Facile synthesis of fluorescence carbon dots from sweet potato for Fe^{3+} sensing and cell imaging. Mater. Sci. Eng. C 76, 856–864.
Shi, L., Chang, D., Zhang, G., Zhang, C., Zhang, Y., Dong, C., Chu, L., Chuang, S., 2019. Co^{2+}detection, cell imaging, and temperature sensing based on excitation-independent green-fluorescent N-doped carbon dots. RSC Adv. 9, 41361–41367.
Singh, A., Mohapatra, P.K., Kalyanasundaram, D., Kumar, Sunil, 2019. Self-functionalized ultra-stable water suspension of luminescent carbon quantum dots. Mater. Chem. Phys. 225, 23–27.
Souza, S.L.D., Chettiar, S.S., Koduru, J.R., Kailasa, S.K., 2018. Synthesis of fluorescent carbon Dots using *Daucus carota* subsp. sativus roots for mitomycin drug delivery. Optik 158, 893–900.
Su, W., Guo, R., Yuan, F., Li, Y., Li, X., Zhang, Y., Zhou, S., Fan, L., 2020. Red-emissive carbon quantum dots for nuclear drug delivery in cancer stem cells. J. Phys. Chem. Lett. 11, 1357–1363.
Sun, Y.P., Zhou, B., Lin, Y., Wang, W., Fernando, K.A.S., Pankaj, Pathak, Meziani, J.M., Barbara, A., Harruff, Wang, X., Wang, H., Luo, P.G., Yang, H., Kose, M.E., Chen, B., Veca, L.M., Xie, S.Y., 2006. Quantum-sized carbon dots for bright and colourful photoluminescence. J. Am. Chem. Soc. 128, 7756–7757.
Sun, X., He, J., Yang, S., Zheng, M., Wang, Y., Ma, S., Zheng, H., 2017. Green synthesis of carbon dots originated from Lycii Fructus for effective fluorescent sensing of ferric ion and multicolour cell imaging. J. Photochem. Photobiol. B Biol. 175, 219–225.
Suresh Kumar, K., Ha, S., Baek, S.H., Phan, L.M.T., Kim, S., Kwak, K., Park, T.J., 2019. Tuning of carbon dots emission colour for sensing of Fe^{3+} ion and bioimaging applications. Mater. Sci. Eng. C 98, 834–842.
Theerthagiri, J., Chandrasekaran, S., Salla, S., Elakkiya, V., Senthil, R.A., Nithyadharseni, P., Maiyalagan, T., Micheal, K., Mariam, A., Valan Arasu, M., Al-Dhabi, N.A., Kim, H.S., 2018. Recent developments of metal oxide-based heterostructures for photocatalytic applications towards environmental remediation. J. Solid State Chem. 267, 35–52.
Vadivel, R., Thiyagarajan, S.K., Raji, K., Suresh, R., Sekar, R., Ramamurthy, P., 2016. Outright green synthesis of fluorescent carbon dots from eutrophic algal blooms for in vitro imaging. ACS Sustain. Chem. Eng. 4, 4724–4731.
Vandarkuzhali, S.A.A., Natarajan, S., Jeyabalan, S., Sivaraman, G., Singaravadivel, S., Muthusubramanian, S., Viswanathan, B., 2018. Pineapple peel-derived carbon dots: applications as sensor, molecular keypad lock, and memory device. ACS Omega 3, 12584–12592.
Wan, Y., Wang, M., Zhang, K., Fu, Q., Gao, M., Wang, L., Xia, Z., Gao, D., 2019. Facile and Green synthesis of fluorescent carbon dots from the flowers of *Abelmoschus manihot (Linn.)* Medicus for sensitive detection of 2,4,6- trinitrophenol and cellular imaging. Microchem. J. 148, 385–396.
Wang, W., Zeng, Z., Zeng, G., Zhang, C., Xiao, R., Zhou, C., Xiong, W., Yang, Y., Lei, L., Liu, Y., Huang, D., Cheng, M., Yang, Y., Fu, Y., Luo, H., Zhou, Y., 2019. Sulfur doped carbon quantum dots loaded hollow tubular g-C_3N_4 as novel photocatalyst for destruction of Escherichia coli and tetracycline degradation under visible light. Chem. Eng. J. 378, 122132.
Wang, W., Chen, J., Wang, D., Shen, Y., Yang Zhang, T., Ge, J., 2021. Facile synthesis of biomass waste-derived fluorescent N, S, P co-doped carbon dots for detection of Fe^{3+} ions in solutions and living cells. Anal. methods 13, 789–795.
Xu, X., Ray, R., Gu, Y., Ploehn, H.J., Gearheart, L., Raker, K., Scrivens, W.A., 2004. Electrophoretic analysis and purification of fluorescent single-walled carbon nanotube fragments. J. Am. Chem. Soc. 126, 12736–12737.
Yang, X., Zhou, Zhu, S., Luo, Y., Feng, Y., Yao, 2014. Novel and green synthesis of high-fluorescent carbon dots originated from honey for sensing and imaging. Biosens. Bioelectron. 60, 292–298.
Yue, L., Li, H., Liu, Q., Guo, D., Chen, J., Sun, Q., Xu, Y., Wu, F., 2019. Manganese-doped carbon quantum dots for fluorometric and magnetic resonance (dual-mode) bioimaging and biosensing. Microchimica Acta 186, 315.
Zhan, J., Peng, R., Wei, S., Chen, J., Peng, X., Xiao, B., 2019. Ethanol-precipitation-assisted highly efficient synthesis of nitrogen-doped carbon quantum dots from chitosan. ACS Omega 4, 22574–22580.
Zhang, Y., Gao, Z., Yang, X., Chang, J., Liu, Z., Jiang, K., 2019. Fish-scale-derived carbon dots as efficient fluorescent nanoprobes for detection of ferric ions. RSC Adv. 9, 940–949.
Zhao, C., Li, X., Cheng, C., Yang, Y., 2019. Green and microwave-assisted synthesis of carbon dots and application for visual detection of cobalt(II) ions and pH sensing. Microchem. J. 147, 183–190.
Zhao, S., Song, X., Chai, X., Zhao, P., He, H., Liu, Z., 2020. Green production of fluorescent Carbon quantum dots based on pinewood and its application in the detection of Fe^{3+}. J. Clean. Prod. 263, 121561.
Zheng, Y., Wang, Z., Peng, F., Fu, L., Mexicana de, R., 2016. Biosynthesis of silver nanoparticles by Plectranthus amboinicus leaf extract and their catalytic activity towards methylene blue degradation. Ingen. Quim. 16, 41–45.
Zhou, J., Ge, M., Han, Y., Ni, J., Huang, X., Han, S., Peng, Z., Li, Y., Li, S., 2020. Preparation of biomass-based carbon dots with aggregation luminescence enhancement from hydrogenated rosin for biological imaging and detection of Fe^{3+}. ACS Omega 5, 11842–11848.
Zhu, Z., Yang, P., Chen, M., Zhang, T., Cao, Y., Zhang, W., Zhou, X., Chen, W., 2019. Microwave synthesis of amphiphilic carbon dots from xylose and construction of luminescent composites with shape recovery performance. J. Lumin. 21, 474–481.